Quantum-Chemical Investigation of Snow - Mercury Interactions and their Implication of Mercury Deposition in the Arctic

Emaan Ali, 1,2 Nandini Patel, 2 Shrina Patel 2 and Abu Asaduzzaman 2,*

¹Department of Chemical Engineering, Pennsylvania State University – University Park, PA 16802, USA

²School of Science, Engineering and Technology, Pennsylvania State University – Harrisburg, Middletown, PA 17057, USA

*Email: aua1309@psu.edu

Abstract: Elemental gaseous Hg is emitted into the atmosphere through various anthropogenic and natural processes. Its different species and respective transport ranges, atmospheric physical and chemical transformations, and interaction with Earth's surfaces all contribute to the global cycling of toxic mercury. Under the sunlight, halogens, ozone, and nitro species oxidize the emitted elemental Hg to gaseous Hg (II) molecules, which deposit on the snow and ice surfaces in the Arctic. To investigate the fate of deposited mercury, a quantum-chemical investigation was conducted using first-principles density functional theory (DFT) to analyze the interaction between various mercury molecules and snow clusters of differing sizes. Results show all oxidized mercury molecules: XHgY, BrHgOX, BrHgXO XHgOH, XHgOQ2H, XHgNO2, with X, Y = Cl, Br, I atoms have thermodynamically stable interactions with snow clusters. Further, the adsorption energy of all mercury molecules increases with increasing size of snow clusters. Additionally, the orientations of deposited mercury molecules on the cluster surface also influence the mercury-snow interactions.

Introduction

Mercury is a neurotoxic and environmental contaminant. ^{1–12} In recent years, there has been a rising concern over the health of marine life and the northern human population due to reports of increasing atmospheric mercury content in the Arctic.¹³ Introduction of mercury into the atmosphere originates from natural and anthropogenic sources. Natural geological emissions of mercury results from volcanic eruptions and forest fires. Contrastingly, anthropogenic emissions are due to waste incineration, oil and coal combustions, cement production, and pyrometallurgical processes.^{8,14} According to United Nations Environment Program, there is approximately 6000 tons of mercury in the atmosphere. 15 Mercury is released into the atmosphere primarily as gaseous elemental mercury (GEM), also known as Hg(0) although some gaseous Hg(II), referred to as gaseous oxidized mercury (GOM) is also released. 16 GEM has a low water solubility, is less reactive, and has an atmospheric lifetime of 0.5 to 1.7 years. 17 By contrast, GEM has a lifetime of a few days to weeks. Due to its high water solubility and low vapor pressure, Hg(II) can easily partition onto aerosols, is hygroscopic, and is susceptible to wet or dry deposition to surface environments. 18,19 The long lifetime of Hg(0) leads to Hg deposition far from its emission sources to remote ecosystems such as open oceans and polar regions. Once transported to the Arctic, Hg undergoes rapid oxidation and deposition during Atmospheric Mercury Depletion Events

(AMDEs) during the spring season, first reported by Schroeder et al.^{9,20,21} While gas phase O₃, OH, HO₂, H₂O₂, and NO₃ are all potential Hg(0) oxidants, atomic bromine is strongly suggested to initiate Hg(0) oxidation in marine boundary layers and during atmospheric depletion events in Polar regions.^{22–27} The oxidation process under atmospheric conditions is initiated photolytically under a two-step mechanism.^{25,28}

In the first step of the oxidation process, photochemically generated Br atoms form HgBr·, a radical Hg(I) intermediate. This radical can readily compose back to Hg(0) or further be oxidized to Hg(II) compounds by prominent atmospheric radicals such as HO₂, Br, NO₂, OH, I, Cl, BrO, ClO, and IO. Dibble et al.²⁸ proposed that the addition of BrHg• to these radicals dominates the atmospheric fate of BrHg•.

$$Hg + Br \leftrightarrow HgBr \xrightarrow{+X} BrHgX$$

As a result of oxidation by reactive bromine species, AMDE leads to the deposition of ~300t mercury per year in the Arctic. Although AMDEs are mainly responsible for Hg sources in the Arctic, numerous studies suggest that a major fraction of atmospheric depleted mercury is reemitted to the atmosphere following deposition onto snowpack.^{29–35} However, the remaining mercury can potentially move to deeper layers of snowpack as snow serves as a natural sink for trace elements.^{36,37} Once deposited, mercury converts into methylmercury through the process of methylation from microbial activity present in the water.^{30,38–43} This toxic form of mercury can potentially result in impaired neurological development, headaches, cognitive and motor dysfunction, fatigue, etc.⁴⁴ Arctic indigenous communities are particularly vulnerable to the impacts of these effects in their traditional/local foods.¹³ As a result of the threatening impacts of mercury emissions, the international community in 2013 signed a treaty at the Minamata Convention agreeing to reduce mercury emissions to safe levels. Currently, numerous extensive studies are being conducted to understand the biogeochemical cycle of mercury to implement the Minamata Convention. However, attaining this goal is difficult as mercury rapidly oxidizes in AMDEs and re-emits from surface ecosystems back into the atmosphere.

Nevertheless, researchers attempting to understand this cycle lack basic information on the kinetics and mechanisms of AMDEs. This lack of sufficient data undermines the effort to synthesize models of the global chemistry of mercury. The main difficulties in experimental studies lie in reproducing the natural air-surface interaction or changing controlling factors in the lab. Further, experimental research is complex due to mercury's neurotoxic effects, ultra-trace concentrations, and complex diversity of its chemical speciation. In general, the continual development of quantum chemical computational modeling has reached the point where it can inform environmental science or even replace difficult experimental investigations. Advances in quantum chemistry calculations have enabled researchers to study interactions between mercury and other particles down to the atomic level. 16,22,24,45–57 Therefore, the primary goal of this investigation is to gain insight into the air-snow-ice-mercury cycling at the atomic level by analyzing the interactions of various potential oxidized mercury molecules with snowpack and ice. The study is carried out with progressively increasing size of snow and ice: from the snow clusters to the ice surface. While the results from mercury - ice surface is published elsewhere, 58

this study is solely focused on the snow clusters. Specifically, we have aimed to investigate the cluster size dependent mercury interactions.

Computational Methods

All calculations were performed using electronic structure density functional theory (DFT) using plane wave basis sets as implemented in the software VASP (Vienna ab initio simulation package) version 5.4.1. 59,60 The exchange-correlation contribution to the total energy is modeled using the generalized-gradient approximation (GGA) functional. The orbital interactions are analyzed by projector-augmented-wave method (PAW), 61 specifically utilizing Perdew-Burke-Ernzerhof (PBE) 62 pseudopotentials provided by VASP. Using pseudopotentials ensures a scalar relativistic approach is included in the calculations. The energy cutoff was set to 500 eV to maximize the completeness of the planewave basis sets. The Monkhorst-Pack k-point 63 grid was set to gamma point only and applied to both the individual compounds and combined snow structures calculations. The convergence criterion for local energy minima is that all atomic forces be smaller than 0.02 eV/Å. All calculations were performed using the supercell approach using a simulation box of $30 \text{ Å} \times 30 \text{ Å} \times 30 \text{ Å}$.

Snow, a single crystal of ice appears on a scale of hundreds of microns or even millimeters with varying shapes. Modeling such snow structures using ab initio quantum chemistry is, thus, a very challenging task. However, nanometer sized clusters, which are considered in this study are many orders magnitude smaller than typical snow and can be generated from both snow and ice. Therefore, we have generated them by curving out spherical clusters from regular hexagonal ice crystals. Centering at an oxygen atom of a water molecule of bulk ice, the radius of a spherical part of the ice is progressively increased and curved out from the bulk ice. In generating these clusters, we chose only those clusters with no H-O bonds in a water molecule are broken, i.e., only the hydrogen bonds between two different water molecules are broken. It also ensures the stoichiometry of water in snow clusters. The number of water molecules in our modeled snow clusters are 5, 12, 39, and 73. For each cluster, the structures are optimized to their local energy minima. Similarly, twenty-seven mercury molecules are optimized at their local energy minima using the same computational protocol described above.

Several studies on water clusters^{65–67} and mercury molecules^{68,69} investigated using DFT. In all those studies, atom centered-basis sets were used. On the other hand, we have used plane wave basis set in this study to keep the consistency between mercury - cluster and mercury - surface interactions.⁵⁸ In addition, such method is successfully employed in our previous studies^{70–72} involving ice.

Results and Discussion

Our investigation begins with the optimization of individual mercury compounds. Although some combinations have been experimentally shown in numerous studies, various compounds³⁸ were tested to investigate the possibility of mercury deposition on the surface. Figure 1 presents the structures of oxidized mercury molecules. The optimized structural parameters and Cartesian coordinates of all mercury molecules are listed in Table S1 and S2, respectively. Each oxidized mercury compound is composed of a halogen (X) anion and an oxide, or a secondary halogen

atom as the second anion. Based on these structural and compositional differences, the compounds are classified into four distinct categories: (a) mercury – halides (HgX_2), (b) mercury - oxyhalides/halo oxides (XHgOX/XHgXO) (c) mercury - hydrogen oxides (XHgOH and XHgO₂H) and (d) mercury – nitrogen oxides (XHgNO₂). Based on the structural arrangements, XHgNO₂ compounds are classified into three subcategories: (i) XHgNO₂ (Figure 1(e)), where Nitrogen connects to Hg; (ii) syn-XHgNO₂, where Oxygen connects to Hg, and the O-N-O linking is on the same side of Hg (Figure 1(d)); and (iii) anti-XHgNO₂, where O connects to Hg and the O-N-O linking is on the opposite side of Hg (Figure 1(f)). Each mercury compound was individually optimized to obtain its lowest energy geometry for placement on each snow cluster. The structural parameters, specifically the bond distances between Hg and X/O/N were reported in numerous studies. 38,51,55,56,73-77 The level of theory, exchange-correlation functionals, basis sets, spin-orbit couplings all have an impact on the structural parameters of mercury molecules. Generally, higher level of theory, e.g., CCSD(T) and higher basis sets result in the shortening of bond distances in Hg-X/O/N.55,75 Our calculated bond distances and bond angles for optimized mercury molecules are within 2% of the corresponding literature values. It is to be noted that BrHgXO molecules are not reported experimentally and are significantly less stable than corresponding BrHgOX molecules.^{38,74} However, Jiao and Dibble⁷⁴ showed by very high level computational methods that BrHgIO will be thermally stable in the Arctic atmosphere. On the other hand, BrHgBrO has a lifetime of 20h, which is sufficient to be adsorbed on snow/ice surface during ADMEs, which typically last a few hours to a day. The unstable compound is BrHgClO (lifetime is 0.4h). However, for the sake of complementing all other mercury compounds, BrHgClO is also considered in this study.

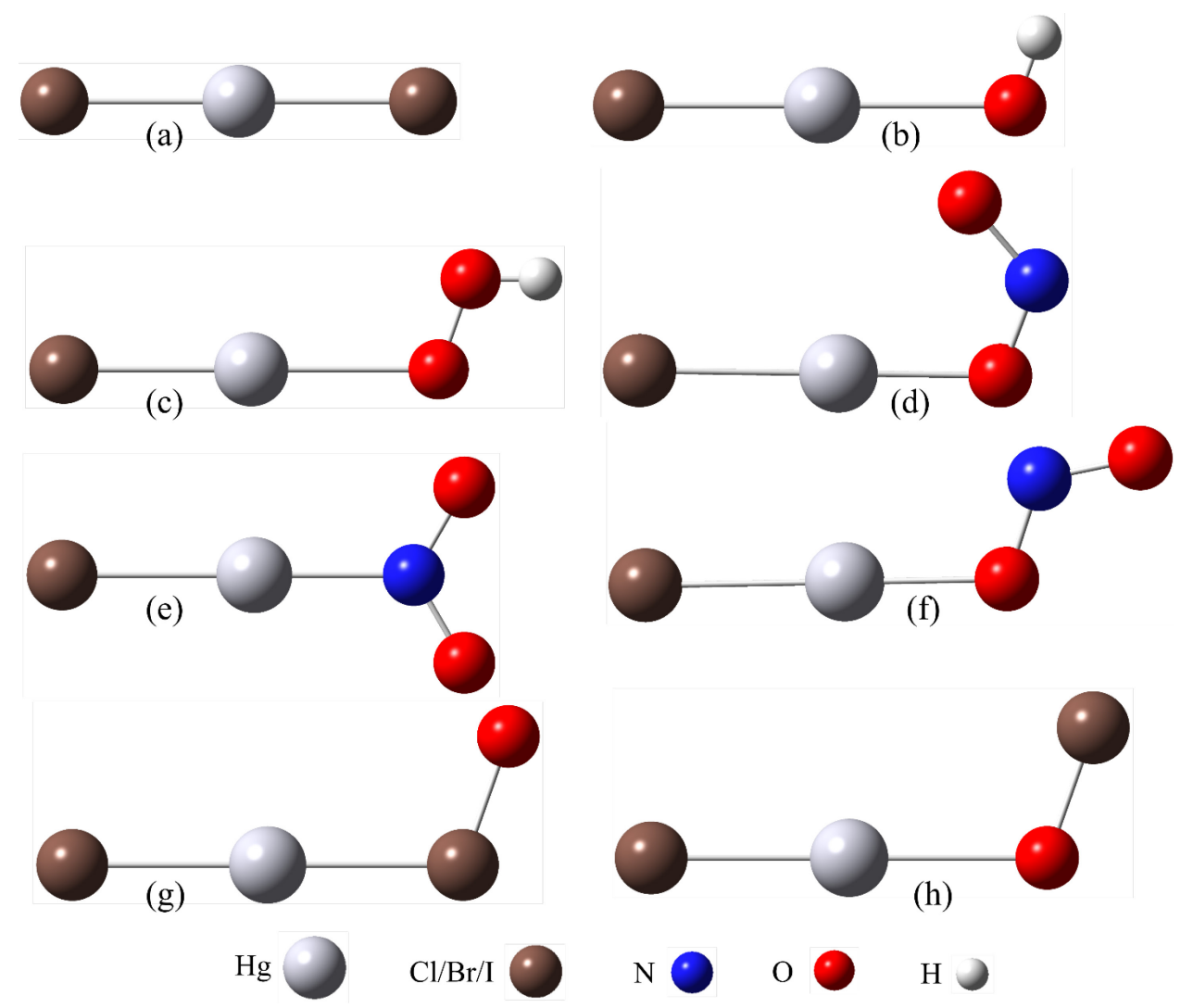


Figure 1. Ball and stick presentation of oxidized mercury molecules: (a) halides; (b) XHgOH; (c) $XHgO_2H$; (d)SYN-XHgONO; (d) $XHgNO_2$; (f) anti-XHgONO; (g) SYN-XHgONO and (h) SYN-XHgONO with SYN-XHgONO; (e) SYN-XHgONO; (f) anti-SYN-XHgONO; (g) SYN-XHgONO; (h) SYN-XHgONO; (g) SYN-XHgONO; (e) SYN-XHgONO; (f) anti-SYN-XHgONO; (g) SYN-XHgONO; (h) SYN-XHgONO; (e) SYN-XHgONO; (f) SYN-XHgONO; (f) SYN-XHgONO; (g) SYN-XHgONO; (e) SYN-XHgONO; (f) SYN-XHgONO; (f) SYN-XHgONO; (g) SYN-XHgONO; (e) SYN-XHgONO; (f) SYN-XHgONO; (g) SYN-XHgONO

Secondly, we have optimized four snow clusters with different sizes and a single water molecule in the same cubic box. The optimized structures of all clusters are presented in Figure 2. The optimized coordinates (CONTCAR files) for all four clusters are in Table S3. Although all clusters are generated by curving out a spherical part from the ice crystal, the surface structures of each cluster are different. 5-water cluster is a tetrahedral arrangement of four water molecules around a central water (Fig. 2a). The 12- and 39-water clusters have flat surface structures like the (0001) surface of ice, see Fig. 2(b) and (c). Lastly, the 73 cluster is more spherical and less flat.

The binding energy per water molecule in each snow cluster is calculated using equation (1).

$$\Delta E_b = \frac{E_n - n.E_{water}}{n} \dots (1)$$

 E_n is the total energy of a cluster with n water molecules, n = 5, 12, 39 and 73, and E_{water} is the energy of a single water molecule in the gas phase. The binding energy of each cluster versus the number of water molecule is plotted in Figure 3.

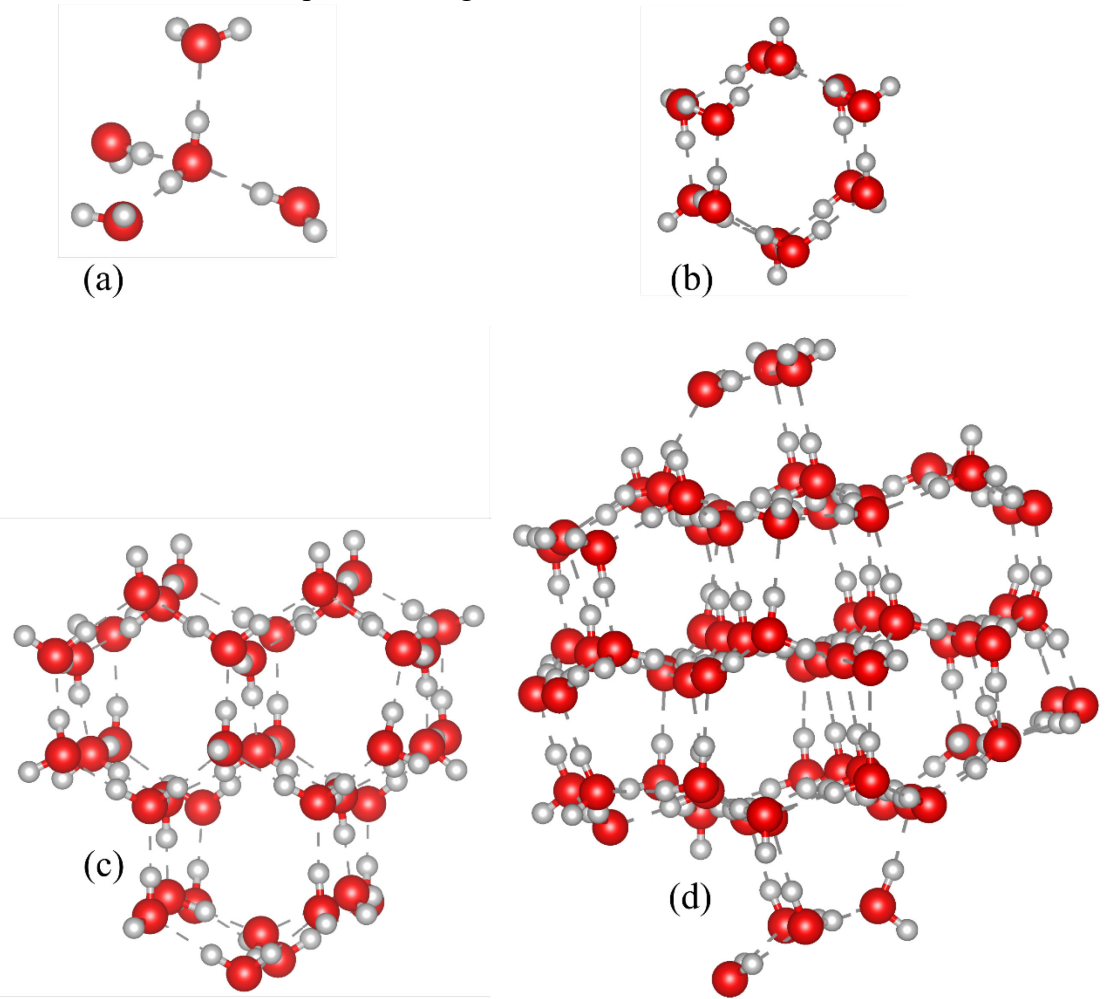


Figure 2. Optimized snow clusters with (a) 5 (b) 12 (c) 39 (d) 73 water molecules. Red and white spheres represent O and H atoms, respectively.

The binding energy of the cluster decreases with increasing the number of H₂O units, as shown in Figure 3. In other words, as the cluster size increases, the binding energy decreases due to its higher stability as the surface-to-bulk ratio decreases, which coincides with previous TiO₂ clusters and water clusters.^{78–80} It is expected that with larger clusters, the binding energy converges to that of the bulk ice. Structurally, a few water molecules of the clusters move to the center of the hexagon as shown in Figure 2(d). Further, structures and energetics of water clusters were previously reported.^{65,66,79–81} Using DFT and tight binding DFT along with atom centered basis sets, those studies had focused on the structures, symmetries, and energetics of water clusters. Specifically, they used a bottom-up approach by increasing one water molecule in successive cluster starting from a single water molecule. Many different isomers for each cluster were considered, especially for small clusters.⁷⁹ However, for the larger clusters the number of isomers were limited.^{79,80} The binding energy for those water clusters were varied depending on the computational methodology. On the other hand, we have generated all clusters by curving out

a spherical part of crystalline ice. Therefore, there is only one isomer for each cluster in this study. Furthermore, the focus of our study is the interaction between clusters and mercury molecules as opposed to the stability and binding energy of water clusters in those previous studies. Nevertheless, we have validated our methodology by calculating the binding energy of one water cluster reported in the literature.^{66,79} The binding energy for fused tetrameric 12 water cluster was reported 119 kJ/mol at DFT/M06-L level of theory by Miró and Cramer.⁶⁶ The binding energy of the same cluster was reported respectively as 124.7, 130.1, 119.5 and 121.4 kJ/mol at M06-2X/aVTZ, APFD/aVTZ, MN15/aVTZ and ωB97XD/aVTZ level of theory.⁷⁹ On comparison, our calculated binding energy for the same cluster is 124.6 kJ/mol, which is within the reported value. The agreement of our calculated binding energy with literature values provided with the validation of our calculated results.

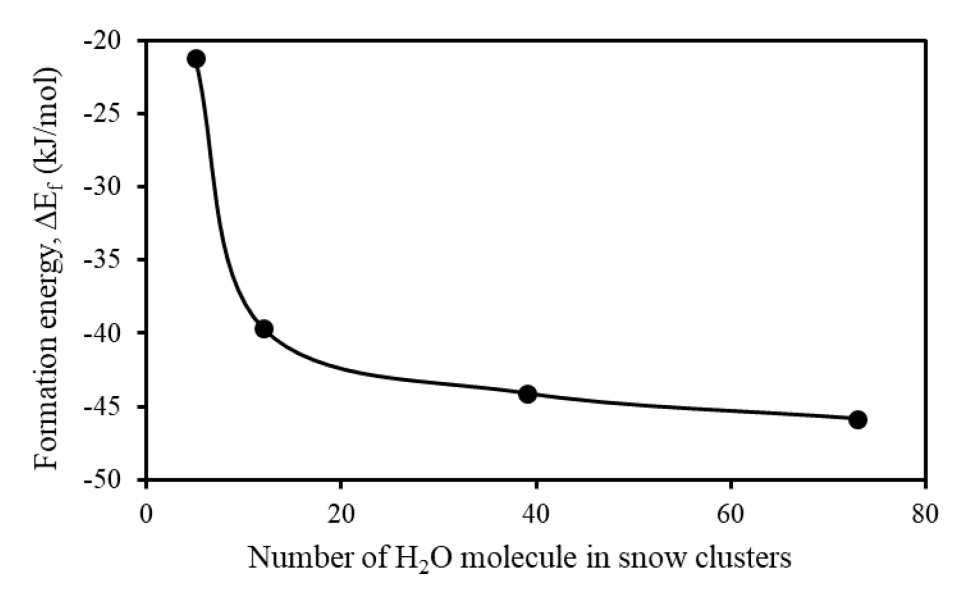


Figure 3. Formation energy, ΔE_f (kJ/mol)(uncorrected zero-point energy) of snow cluster with cluster size.

Adsorption or interaction energy of mercury molecules on snow cluster is calculated using equation (2).

$$\Delta E_{ad} = E_{HS} - (E_H + E_S) \dots (2)$$

 E_{HS} refers to the calculated total energy of the mercury molecules with snow cluster. Contrastingly, E_{H} and E_{S} denote the energy of the individual mercury molecules and the energy of the snow cluster, respectively. The negative value of adsorption energy indicates stable adsorption of mercury molecules on the snow surface and vice versa. However, for the sake of simplicity only numerical values are used to qualitatively describe the adsorption or interaction. For example, $\Delta E_{ads} = -100 \text{ kJ/mol}$ is referred as higher adsorption energy than $\Delta E_{ads} = -90 \text{ kJ/mol}$.

Following the optimization of mercury molecules and snow clusters, each oxidized mercury molecule is laid on the optimized cluster surfaces. The cluster-mercury molecule structures were then optimized at their lowest local energy minima. Oxidized mercury molecules are laid on the snow clusters in two positions: (a) parallel and (b) perpendicular. For perpendicular orientation, the O/N atom connections to the snow cluster result in stronger

interactions as opposed to halogen connections to the cluster surface. Therefore, results from the N/O connections are presented in this manuscript. The optimized coordinates (CONTCAR files) for all snow-mercury structure are available in Table S4. Figures 4 and 5 below present the optimized structures for the BrHgOH molecule positioned parallel and perpendicularly on all clusters. The structures of mercury molecules on the snow clusters are very similar to those of Fig. 4 and 5. The primary interactions between mercury molecules and snow clusters are the hydrogen bonds as can be seen in the distances between molecules and clusters in Figs. 4 and 5. Such hydrogen bonds result the adsorption energy is in the same range of typical hydrogen bonds. It is to be noted that due to the spherical shape of clusters, the mercury molecules could be laid on the cluster multiple ways, and therefore, many different local energy structures for snow-mercury interactions are possible. To investigate this, we have laid the BrHgOBr molecule on the 12-water cluster in 5 more ways and optimized them at their local energy minima. The adsorption energies (-16.6 to -3.6 kJ/mol; see Figure S1) for those 5 orientations of BrHgOBr are within in the values for parallel and perpendicular orientations (see Table 1). This finding provides us the hint that adsorption energies for the parallel and perpendicular orientations are on the two opposite sides of the spectrum for adsorption. For the smaller clusters, there may be more orientations for other molecules. However, as the clusters grow bigger, the adsorption energy in the parallel orientation will be the dominant mode for adsorption, like on the (0001) surface⁵⁸ as more flat surfaces for larger clusters are expected. Further, we have considered two 12-water clusters from Miró and Cramer⁶⁶ for the adsorption of BrHgOH. The calculated adsorption energies for BrHgOH in parallel orientation on those two clusters are 26.0 and 27.0 kJ/mol, which are closed to the values for our spherical clusters.

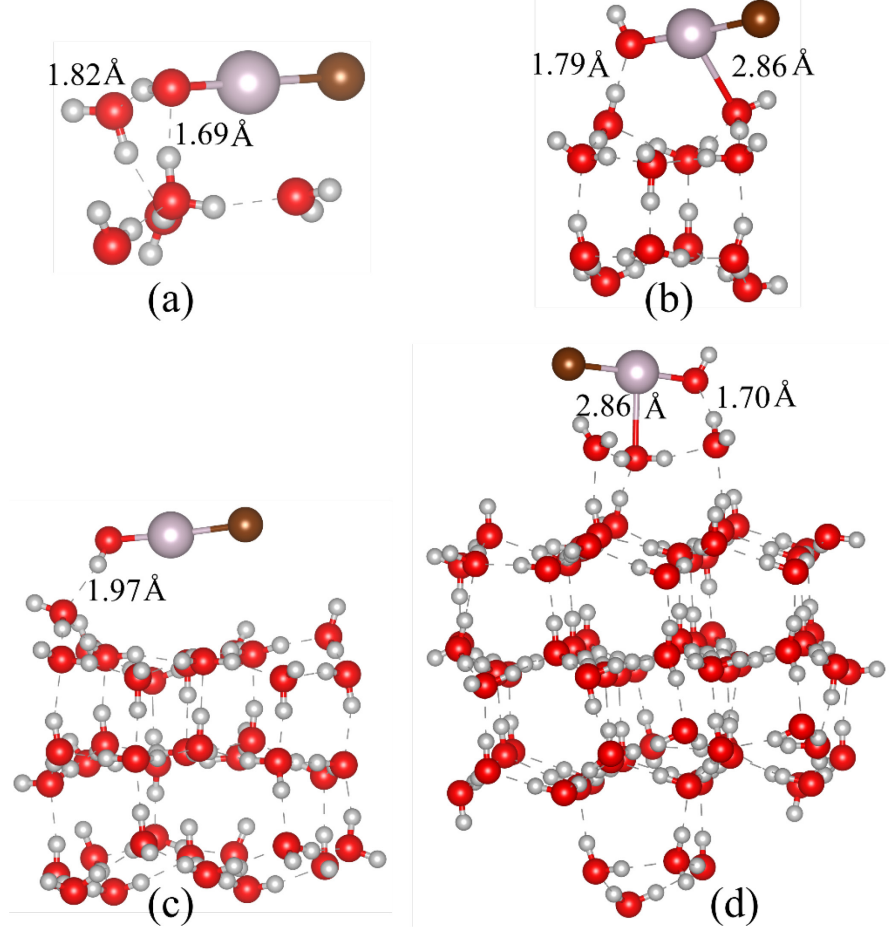


Figure 4. Optimized parallel orientation of BrHgOH on (a) 5 (b) 12 (c) 39 (d) 73 water snow clusters. The presentation is as of Figure 1 and 2. The distances between molecules and snow cluster are shown.

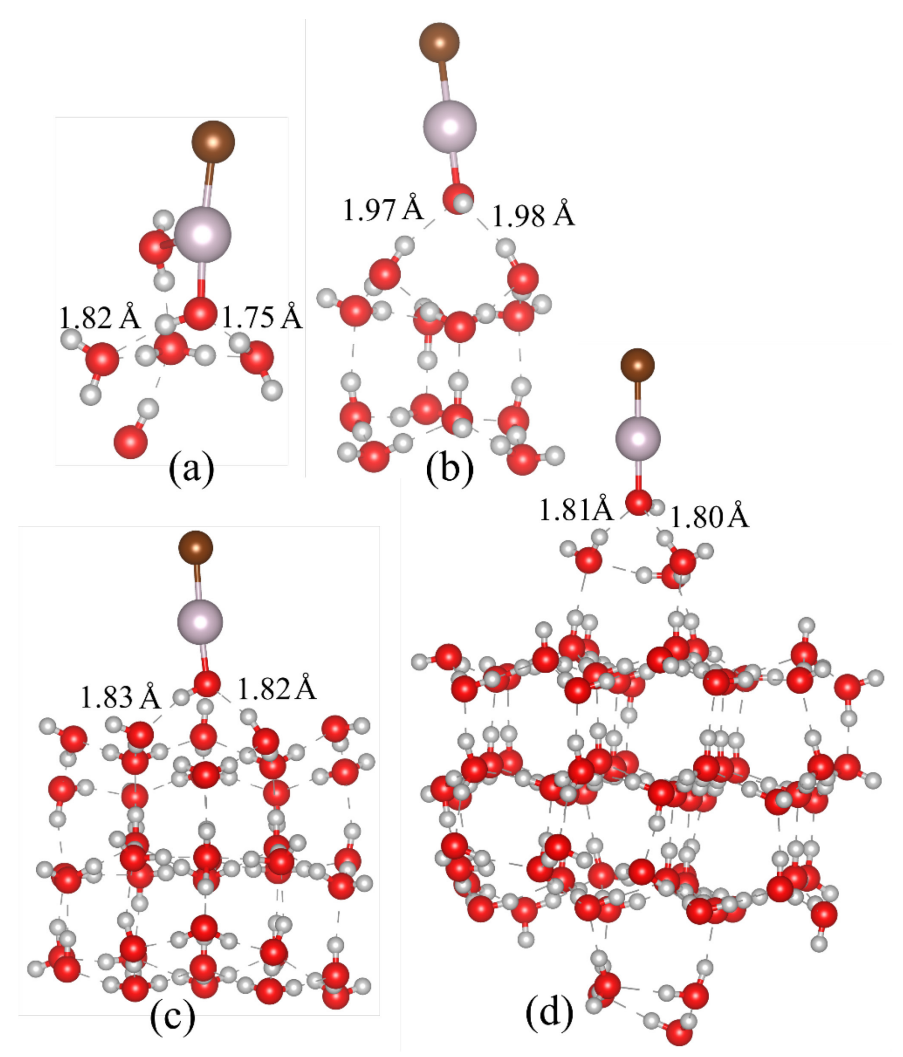


Figure 5. Optimized perpendicular orientation of BrHgOH on (a) 5 (b) 12 (c) 39 (d) 73 water snow clusters. The presentation is as of Figures 1,2 and 4. The distance between BrHgOH and cluster is also shown.

The adsorption energies for molecules on all snow clusters are summarized in Table 1.

Table 1. Adsorption energy, ΔE_{ads} (kJ/mol) of mercury molecules on the snow clusters of different sizes (5, 12, 39 and 73 water molecules). = and \perp respectively represent parallel and perpendicular orientations of mercury molecules.

Adsorption energies, ΔE_{ads} (kJ/mol)												
Cluster size →	5		12		39		73					
Molecules ↓	=	1	=	上	=	Т	=	工				
BrHgClO	-82.6	-82.5	-111.4	-28.8	-83.3	-71.0	-89.4	-108.6				
BrHgBrO	-111.9	-53.4	-118.2	-32.4	-105.4	-72.0	-92.7	-59.7				
BrHgIO	-244.4	-235.6	-211.9	-185.2	-225.3	-230.6	-271.5	-263.9				
BrHgOCl	-51.5	-25.4	-16.9	-9.2	-55.7	-57.6	-61.3	-47.0				
BrHgOBr	-40.8	-26.3	-17.9	-5.4	-54.4	-60.3	-64.2	-77.1				
BrHgOI	-52.2	-31.0	-18.9	-6.1	-55.4	-111.4	-66.0	-79.9				

ClHgNO ₂	-35.1	-76.8	-29.3	-6.5	-51.9	-59.5	-54.9	-53.9
anti-ClHgONO_	-66.9	-46.2	-21.6	-11.7	-51.4	-50.4	-51.3	-63.6
syn-ClHgONO	-67.3	-72.1	-27.5	0.4	-41.1	-52.0	-55.1	-61.1
BrHgNO ₂	-34.8	-74.6	-34.9	-3.2	-52.6	-60.9	-54.0	-51.2
anti-BrHgONO	-57.5	-68.3	-29.1	-3.2	-54.0	-86.4	-48.1	-65.8
syn-BrHgONO	-46.7	-67.5	-32.2	-0.3	-47.4	-51.8	-53.9	-62.8
IHgNO ₂	-34.5	-65.4	-16.8	-10.1	-48.3	-49.0	-55.8	-56.4
anti-IHgONO	-42.3	-42.2	-25.2	-12.2	-68.1	-52.5	-45.6	-68.8
syn-IHgONO	-45.1	-68.2	-12.9	-0.9	-45.2	-54.4	-48.7	-67.1
BrHgO ₂ H	-87.2	-70.0	-35.5	-52.5	-79.8	-86.9	-81.9	-77.0
ClHgO ₂ H	-82.8	-80.9	-29.3	-52.0	-81.3	-88.1	-86.8	-75.6
IHgO ₂ H	-86.3	-81.2	-29.3	-52.8	-90.3	-90.7	-80.4	-81.1
ClHgOH	-75.7	-77.3	-30.3	-40.8	-82.0	-66.3	-67.9	-62.0
BrHgOH	-65.1	-68.3	-25.5	-30.7	-48.4	-70.8	-68.9	-67.8
IHgOH	-75.7	-71.6	-25.9	-40.3	-51.3	-70.1	-63.8	-73.9
HgCl ₂	-20.7	-23.6	-12.6	-6.0	-54.4	-44.0	-56.1	-44.1
$HgBr_2$	-42.4	-20.5	-11.1	-5.8	-51.7	-43.8	-53.9	-44.9
HgI_2	-15.2	-23.2	-12.8	-4.9	-53.4	-47.9	-51.7	-47.2
BrHgCl	-21.0	-20.7	-13.4	-6.6	-55.3	-46.8	-56.0	-48.0
ClHgI	-22.9	-34.6	-13.4	-9.5	-51.6	-49.4	-53.2	-55.3
BrHgI	-17.7	-22.5	-10.3	-7.6	-53.9	-46.5	-51.9	-48.6

Adsorption of mercury molecules on the cluster surface depends on the Hg-O(surface), H-O(surface), and X/O/N-H(surface) interactions. Due to differences in interatomic distances and orientations, the adsorption energy of mercury molecules varies with structural and compositional differences as can be seen in Table 1. While no trend is observed for weaker adsorption, the adsorption is stronger in parallel orientation than in the perpendicular orientation for stronger adsorption ($\Delta E_{ads} = -30 \text{ kJ/mol}$ and lower) for most cases. In fact, for surface adsorption, the parallel orientation is stronger than perpendicular orientation of all mercury molecules. To evaluate the orientational and structural dependency, adsorption energy is averaged for each class of mercury molecules for both parallel and perpendicular orientations. For example, adsorption energy of BrHgO₂X in parallel orientation is the average of adsorption energies of BrHgO₂Cl, BrHgO₂Br and BrHgO₂I in parallel orientation. Such average energy for all molecules on all snow clusters is presented in Figure 6.

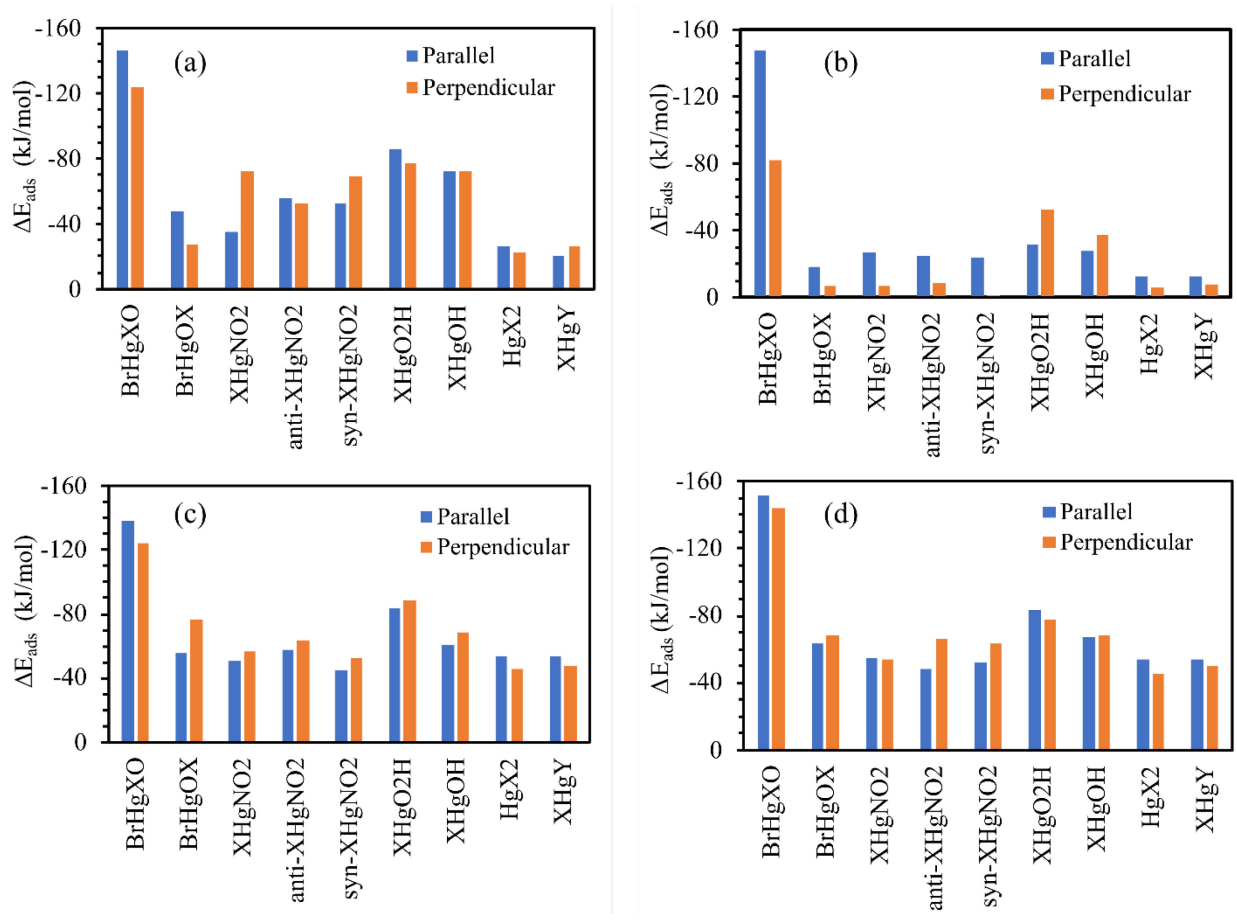


Figure 6. Average adsorption energy, ΔE_{ads} (kJ/mol) of mercury molecules both for parallel and perpendicular adsorption on (a) 5, (b) 12, (c) 39 and (d) 73 water snow clusters. X and Y are halogen atoms. The numeric in the formula of mercury molecules in the x-axis should be read as subscript; for example, XHgNO2 should be read as XHgNO₂.

Although the adsorption energy of parallel and perpendicular orientations differs slightly, there is no significant pattern observed. To start, the adsorption of oxyhalides and halo-oxides to the snow surface in parallel orientation is more stable (has a higher adsorption energy) than that in perpendicular orientation. On the other hand, the adsorption for nitrogen oxides and hydrogen oxides is slightly less stable in parallel orientation than in perpendicular orientation.

Additionally, halide molecules possessed the lowest adsorption energies amongst all molecular groups on the clusters due to the absence of oxygen atom, which could form hydrogen bonds with surface hydrogen. Adsorption energy for mercury molecules varies widely due to the surface structures of clusters and mercury molecules' structures. Ice is a low-density crystal structure with large empty spaces. For example, the distance between two surface hydrogens on a snow cluster is above 4.5 Å. Likewise, surface structures of optimized clusters are different for different clusters. Therefore, adsorbing mercury molecules on those clusters result in different types of interactions, thus varying adsorption energy. However, an important feature to note is that oxygen atoms from mercury molecules lead to stronger interaction through a O-H surface bond as opposed to halogen or hydrogen atoms (e.g., BrHgXO has stronger adsorption that

BrHgOX, see Table 1). Taamalli and co-workers 82 reported the reaction enthalpies between a water molecule and BrHgOH, BrHgO₂H, BrHgNO₂, syn-BrHgONO and anti-BrHgONO using three different level of theory, ω B97X-D/aug-cc-pVTZ, DK-CCSD(T)/ANO-RCC-Large and DK-CCSD(T)-cf/ANO-RCC-Large. The one-to-one comparison of our calculated values to those are not compatible as optimized structures are not the same. However, to provide the validation of our computed adsorption energy, we have calculated the hydration energy of BrHgOH_1wa structure from Taamalli and co-workers. Our calculated hydration energy of -27.9 kJ/mol at PBE level of theory compares well with their corresponding value of -28.3 kJ/mol at the DK-CCSD(T)/ANO-RCC-Large level of theory.

After finding the different adsorption energies for various molecules on each snow cluster, we analyzed the data by averaging the adsorption energy for both parallel and perpendicular orientations for each class of molecules. For example, adsorption energy of BrHgO₂X is calculated by averaging adsorption energies of BrHgO₂Cl, BrHgO₂Br and BrHgO₂I both in parallel and perpendicular orientations. The average adsorption energy for each class of molecule is plotted against the cluster size and presented in Figure 7. The standard deviation for the average adsorption energy is shown in Table S5.

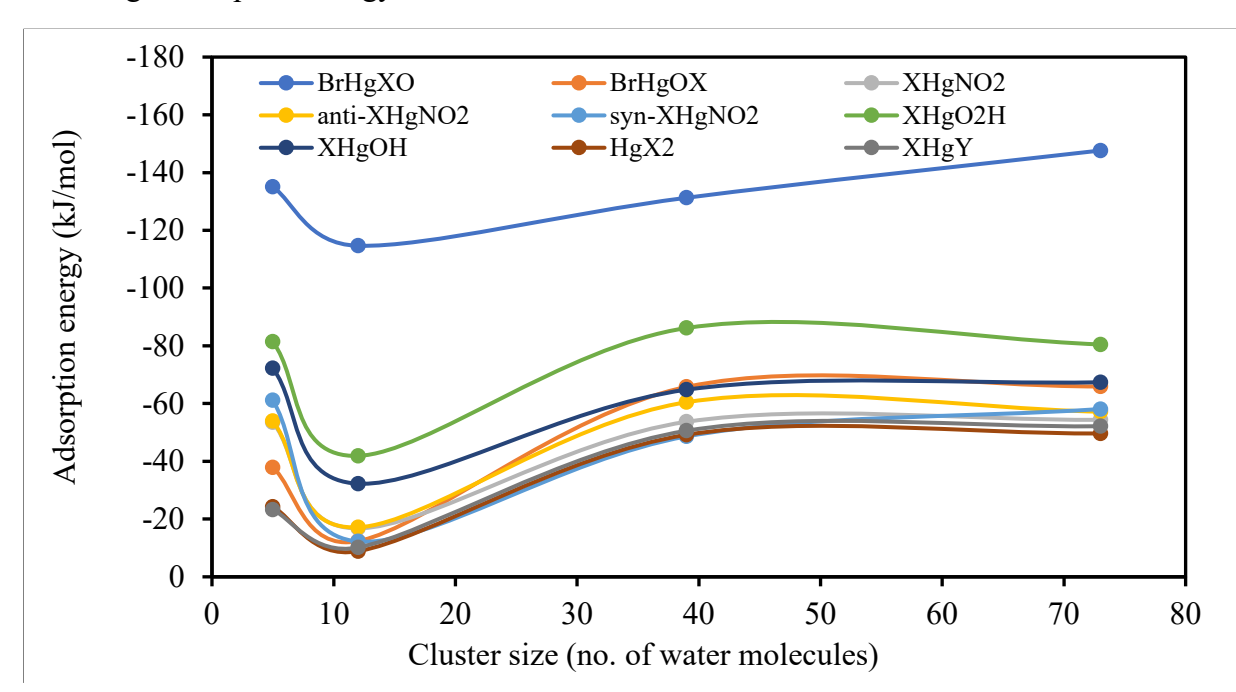


Figure 7. Average adsorption energy (kJ/mol) for each class of mercury molecules with cluster size. X, Y = Cl, Br, I; $X \neq Y$. The numeric in the legend should be read as subscript; for example, XHgO2H should be read as $XHgO_2H$.

Figure 7 reveals that the adsorption energy generally increases with the cluster sizes, with the exception of the five-water cluster. The increment rate is higher from twelve to thirty-nine clusters, whereas the increment is modest from thirty-nine to seventy-three clusters. For XHgO₂H and anti-XHgNO₂ molecules, the adsorption energy on the seventy-three cluster is slightly lower than that of the thirty-nine cluster. Understandably, molecules with more contact points will have higher adsorption energy with increased flat surface area. The adsorption energy

on the seventy-three cluster is more than that on the thirty-nine-cluster due to the flatter surface of the seventy-three cluster, as seen in figure 2(b)-2(d). On the other hand, the five cluster is so small that the adsorption process works more like a water molecule – mercury molecule interaction than surface – mercury molecule interaction. Such a molecular-level interaction leads to high adsorption energy on five water clusters. Generally, the adsorption energy of mercury molecules on any cluster is much less (3-4 times) than the adsorption energy reported on the ice surface. Such a big difference in adsorption energy is because of the dissociative adsorption of mercury molecules on the ice surface as opposed to the associative or molecular adsorption on clusters. One very important point to note is that the adsorption energy for BrHgXO is much higher than those for the rest of the molecules. This is due to the fact that the relative high energy of the BrHgXO molecules means that reaction/relaxation on the cluster surfaces is able to lower the energy to a greater extent than for more strongly bound molecules. It is likely that some of these molecules may dissociate in the atmosphere before depositing on the surface environment.

The AMDEs or rapid oxidation and deposition of mercury during the springtime in the Arctic revolutionize the understanding of mercury oxidation.³¹ It is reported that the majority (~80%) of deposited mercury is reduced back into the atmosphere. 11 Both deposition and reduction were inferred from the measurement of mercury on the surface environment in the Arctic. Further, it is also reported that a fraction of deposited mercury diffuses⁷⁰ through the ice layer or brine channel and reaches the aquatic environment, where they are converted into methyl mercury by surface reducing bacteria and bioaccumulated into the food web.⁴² However, the exact mechanism for the deposition or diffusion has not been explored experimentally or computationally. This study provides the atomic scale details of mercury deposition on ice surfaces as well as possible routes for mercury reduction. While adsorption energies for the molecules are within 100 kJ/mol, given the subzero temperature in the Arctic, these molecules will stick on the surface, especially on the larger clusters. Further, the adsorption structures of some molecules show a sign of dissociation of mercury molecules on the cluster surfaces. Exploring the adsorption on an ice surface confirms⁵⁸ that most molecules are dissociatively adsorbed on the ice surface. Such dissociation would provide a possible mechanism for mercury reduction and a pathway for mercury bioaccumulation.

IV. Conclusion

The interaction of oxidized mercury on snow clusters is explored using the first-principles density functional theory. The snow cluster is modeled by curving out a spherical part from a hexagonal ice crystal. The snow clusters have 5, 12, 39, and 73 water molecules. The formation energy of a cluster gradually decreases with the size of the clusters as the bulk-to-surface area increases. The interaction energy between oxidized mercury molecules and snow clusters depends on the surface structures of snow clusters and the structures of molecules. However, all molecules show attractive interaction with the interaction energy within 100 kJ/mol apart from BrHgOX, which have adsorption energies over 100 kJ/mol with increasing adsorption with cluster size. Generally, O as a terminal atom in the mercury molecules leads to a stronger interaction with the H atoms of the ice cluster. Structural analysis reveals that some mercury

molecules are dissociated on the cluster surfaces, which provides a hint of dissociation and a possible pathway for the reduction of mercury on an ice surface.

Supporting Information

Structural parameters (bond distances and bond angles) and cartesian coordinates of all optimized mercury molecules, snow clusters, and snow-mercury structures are available in the Supporting Information. Standard deviations of adsorption energy are also available.

Acknowledgements

This work is supported by National Science Foundation under the grant number: CHE - 2137662. Computations for this research were performed at Roar supercomputer of the Institute for Computational and Data Science, Penn State's Cyber Infrastructure. We would also like to acknowledge an anonymous reviewer's insightful valuable suggestions, which greatly help in improving the manuscript.

References

- (1) Chang, L. W. Neurotoxic Effects of Mercury—A Review. *Environ. Res.* **1977**, *14*, 329–373.
- (2) Branco, V.; Aschner, M.; Carvalho, C. Neurotoxicity of Mercury: An Old Issue with Contemporary Significance. In *Advances in Neurotoxicology*.; Aschner, M., Costa, L. G., Eds.; Academic Press, 2021; Vol. 5, pp 239–262.
- (3) Shah, E.; Butler, I.; Mancias, P.; Block, K.; Pérez, C. A. Mercury-Induced Neurotoxicity and Neuroinflammation: A Role for Heavy Metal Intoxication in the Pathogenesis of Autoimmune Diseases of the Nervous System (912). *Neurology* **2020**, *94*, 912.
- (4) Teixeira, F. B.; de Oliveira, A. C. A.; Leão, L. K. R.; Fagundes, N. C. F.; Fernandes, R. M.; Fernandes, L. M. P.; da Silva, M. C. F.; Amado, L. L.; Sagica, F. E. S.; de Oliveira, E. H. C.; Crespo-Lopez, M. E.; Maia, C. S. F.; Lima, R. R. Exposure to Inorganic Mercury Causes Oxidative Stress, Cell Death, and Functional Deficits in the Motor Cortex. *Front. Mol. Neurosci.* **2018**, *11*, 125.
- (5) Abdel Moneim, A. Mercury-Induced Neurotoxicity and Neuroprotective Effects of Berberine. *Neural. Regen. Res.* **2015**, *10*, 881-882.
- (6) Driscoll, C. T.; Mason, R. P.; Chan, H. M.; Jacob, D. J.; Pirrone, N. Mercury as a Global Pollutant: Sources, Pathways, and Effects. *Environ. Sci. Technol.* **2013**, *47*, 4967–4983.
- (7) Lyman, S. N.; Jaffe, D. A. Formation and Fate of Oxidized Mercury in the Upper Troposphere and Lower Stratosphere. *Nat. Geosci.* **2012**, *5*, 114–117.
- (8) Ariya, P. A.; Amyot, M.; Dastoor, A.; Deeds, D.; Feinberg, A.; Kos, G.; Poulain, A.; Ryjkov, A.; Semeniuk, K.; Subir, M.; Toyota, K. Mercury Physicochemical and Biogeochemical Transformation in the Atmosphere and at Atmospheric Interfaces: A Review and Future Directions. *Chem. Rev.* **2015**, *115*, 3760–3802.
- (9) Angot, H.; Dastoor, A.; De Simone, F.; Gårdfeldt, K.; Gencarelli, C. N.; Hedgecock, I. M.; Langer, S.; Magand, O.; Mastromonaco, M. N.; Nordstrøm, C.; Pfaffhuber, K. A.; Pirrone, N.; Ryjkov, A.; Selin, N. E.; Skov, H.; Song, S.; Sprovieri, F.; Steffen, A.; Toyota, K.; Travnikov, O.; Yang, X.; Dommergue, A. Chemical Cycling and Deposition of Atmospheric Mercury in Polar Regions:Review of Recent Measurements and Comparison with Models. *Atmos. Chem. Phys.* **2016**, *16*, 10735–10763.

- (10) Chen, C. Y.; Driscoll, C. T.; Lambert, K. F.; Mason, R. P.; Sunderland, E. M. Connecting Mercury Science to Policy: From Sources to Seafood. *Rev. Environ. Health* **2016**, *31*, 17-20.
- (11) Durnford, D.; Dastoor, A. The Behavior of Mercury in the Cryosphere: A Review of What We Know from Observations. *J. Geophys. Res.* **2011**, *116*, D06305.
- (12) Gustin, M. S.; Amos, H. M.; Huang, J.; Miller, M. B.; Heidecorn, K. Measuring and Modeling Mercury in the Atmosphere: A Critical Review. *Atmos. Chem. Phys.* **2015**, *15*, 5697–5713.
- (13) Lockhart, W. L.; Stern, G. A.; Low, G.; Hendzel, M.; Boila, G.; Roach, P.; Evans, M. S.; Billeck, B. N.; DeLaronde, J.; Friesen, S.; Kidd, K.; Atkins, S.; Muir, D. C. G.; Stoddart, M.; Stephens, G.; Stephenson, S.; Harbicht, S.; Snowshoe, N.; Grey, B.; Thompson, S.; DeGraff, N. A History of Total Mercury in Edible Muscle of Fish from Lakes in Northern Canada. *Sci. Total Environ.* **2005**, *351–352*, 427–463.
- (14) Lyman, S. N.; Cheng, I.; Gratz, L. E.; Weiss-Penzias, P.; Zhang, L. An Updated Review of Atmospheric Mercury. *Sci. Total Environ.* **2020**, *707*, 135575.
- (15) UNEP. Chemicals and Water, Global Mercury Assessment, 2002. https://www.unep.org/resources/report/global-mercury-assessment-2002-0. Accessed on February 6, 2023.
- (16) Zhang, L.; Wang, S.; Wu, Q.; Wang, F.; Lin, C.-J.; Zhang, L.; Hui, M.; Yang, M.; Su, H.; Hao, J. Mercury Transformation and Speciation in Flue Gases from Anthropogenic Emission Sources: A Critical Review. *Atmos. Chem. Phys.* **2016**, *16*, 2417–2433.
- (17) Gworek, B.; Dmuchowski, W.; Baczewska-Dąbrowska, A. H. Mercury in the Terrestrial Environment: A Review. *Environ. Sci. Eur.* **2020**, *32*, 128.
- (18) Li, F.; Ma, C.; Zhang, P. Mercury Deposition, Climate Change and Anthropogenic Activities: A Review. *Front. Earth Sci.* **2020**, *8*, 316.
- (19) Dastoor, A.; Angot, H.; Bieser, J.; Christensen, J. H.; Douglas, T. A.; Heimbürger-Boavida, L.-E.; Jiskra, M.; Mason, R. P.; McLagan, D. S.; Obrist, D.; Outridge, P. M.; Petrova, M. V.; Ryjkov, A.; St. Pierre, K. A.; Schartup, A. T.; Soerensen, A. L.; Toyota, K.; Travnikov, O.; Wilson, S. J.; Zdanowicz, C. Arctic Mercury Cycling. *Nat. Rev. Earth Environ.* **2022**, *3*, 270–286.
- (20) Schroeder, W. H.; Anlauf, K. G.; Barrie, L. A.; Lu, J. Y.; Steffen, A.; Schneeberger, D. R.; Berg, T. Arctic Springtime Depletion of Mercury. *Nature* **1998**, *394*, 331–332.
- (21) Steffen, A.; Douglas, T.; Amyot, M.; Ariya, P.; Aspmo, K.; Berg, T.; Bottenheim, J.; Brooks, S.; Cobbett, F.; Dastoor, A.; Dommergue, A.; Ebinghaus, R.; Ferrari, C.; Gardfeldt, K.; Goodsite, M. E.; Lean, D.; Poulain, A. J.; Scherz, C.; Skov, H.; Sommar, J.; Temme, C. A Synthesis of Atmospheric Mercury Depletion Event Chemistry in the Atmosphere and Snow. *Atmos. Chem. Phys.* **2008**, *8*, 1445–1482.
- (22) Saiz-Lopez, A.; Travnikov, O.; Sonke, J. E.; Thackray, C. P.; Jacob, D. J.; Carmona-García, J.; Francés-Monerris, A.; Roca-Sanjuán, D.; Acuña, A. U.; Dávalos, J. Z.; Cuevas, C. A.; Jiskra, M.; Wang, F.; Bieser, J.; Plane, J. M. C.; Francisco, J. S. Photochemistry of Oxidized Hg(I) and Hg(II) Species Suggests Missing Mercury Oxidation in the Troposphere. *Proc. Natl. Acad. Sci. USA* **2020**, *117*, 30949-30956.
- (23) Auzmendi-Murua, I.; Castillo, Á.; Bozzelli, J. W. Mercury Oxidation via Chlorine, Bromine, and Iodine under Atmospheric Conditions: Thermochemistry and Kinetics. *J. Phys. Chem. A* **2014**, *118*, 2959–2975.

- (24) Saiz-Lopez, A.; Sitkiewicz, S. P.; Roca-Sanjuán, D.; Oliva-Enrich, J. M.; Dávalos, J. Z.; Notario, R.; Jiskra, M.; Xu, Y.; Wang, F.; Thackray, C. P.; Sunderland, E. M.; Jacob, D. J.; Travnikov, O.; Cuevas, C. A.; Acuña, A. U.; Rivero, D.; Plane, J. M. C.; Kinnison, D. E.; Sonke, J. E. Photoreduction of Gaseous Oxidized Mercury Changes Global Atmospheric Mercury Speciation, Transport and Deposition. *Nat. Commun.* **2018**, *9*, 4796.
- (25) Gratz, L. E.; Ambrose, J. L.; Jaffe, D. A.; Shah, V.; Jaeglé, L.; Stutz, J.; Festa, J.; Spolaor, M.; Tsai, C.; Selin, N. E.; Song, S.; Zhou, X.; Weinheimer, A. J.; Knapp, D. J.; Montzka, D. D.; Flocke, F. M.; Campos, T. L.; Apel, E.; Hornbrook, R.; Blake, N. J.; Hall, S.; Tyndall, G. S.; Reeves, M.; Stechman, D.; Stell, M. Oxidation of Mercury by Bromine in the Subtropical Pacific Free Troposphere. *Geophys. Res. Lett.* 2015, 42, 10494–10502.
- (26) Jones, C. P.; Lyman, S. N.; Jaffe, D. A.; Allen, T.; O'Neil, T. L. Detection and Quantification of Gas-Phase Oxidized Mercury Compounds by GC/MS. *Atmos. Meas. Tech.* **2016**, *9*, 2195–2205.
- (27) Wang, F.; Saiz-Lopez, A.; Mahajan, A. S.; Gómez Martín, J. C.; Armstrong, D.; Lemes, M.; Hay, T.; Prados-Roman, C. Enhanced Production of Oxidised Mercury over the Tropical Pacific Ocean: A Key Missing Oxidation Pathway. *Atmos. Chem. Phys.* **2014**, *14*, 1323–1335.
- (28) Jiao, Y.; Dibble, T. S. First Kinetic Study of the Atmospherically Important Reactions BrHg'+ NO₂ and BrHg'+ HOO. *Phys. Chem. Chem. Phys.* **2017**, *19*, 1826–1838.
- (29) Steffen, A.; Bottenheim, J.; Cole, A.; Ebinghaus, R.; Lawson, G.; Leaitch, W. R. Atmospheric Mercury Speciation and Mercury in Snow over Time at Alert, Canada. *Atmos. Chem. Phys.* **2014**, *14*, 2219–2231.
- (30) Beattie, S. A.; Armstrong, D.; Chaulk, A.; Comte, J.; Gosselin, M.; Wang, F. Total and Methylated Mercury in Arctic Multiyear Sea Ice. *Environ. Sci. Technol.* **2014**, *48*, 5575–5582.
- (31) Douglas, T. A.; Loseto, L. L.; Macdonald, R. W.; Outridge, P.; Dommergue, A.; Poulain, A.; Amyot, M.; Barkay, T.; Berg, T.; Chételat, J.; Constant, P.; Evans, M.; Ferrari, C.; Gantner, N.; Johnson, M. S.; Kirk, J.; Kroer, N.; Larose, C.; Lean, D.; Nielsen, T. G.; Poissant, L.; Rognerud, S.; Skov, H.; Sørensen, S.; Wang, F.; Wilson, S.; Zdanowicz, C. M. The Fate of Mercury in Arctic Terrestrial and Aquatic Ecosystems, A Review. *Environ. Chem.* **2012**, *9*, 321-355.
- (32) Carignan, J.; Sonke, J. The Effect of Atmospheric Mercury Depletion Events on the Net Deposition Flux around Hudson Bay, Canada. *Atmos. Environ.* **2010**, *44*, 4372–4379.
- (33) Johnson, K. P.; Blum, J. D.; Keeler, G. J.; Douglas, T. A. Investigation of the Deposition and Emission of Mercury in Arctic Snow during an Atmospheric Mercury Depletion Event. *J. Geophys. Res.* **2008**, *113*, D17304.
- (34) Kirk, J. L.; St. Louis, V. L.; Sharp, M. J. Rapid Reduction and Reemission of Mercury Deposited into Snowpacks during Atmospheric Mercury Depletion Events at Churchill, Manitoba, Canada. *Environ. Sci. Technol.* **2006**, *40*, 7590–7596.
- (35) Ariya, P. A.; Dastroor, A. P.; Amyot, M.; Schroeder, W. H.; Barrie, L.; Anlauf, K.; Raofie, F.; Ryzhkov, A.; Davignon, D.; Lalonde, J.; Steffen, A. The Arctic: A Sink for Mercury. *Tellus B: Chem. Phys. Meteor.* **2004**, *56*, 397–403.
- (36) Sun, R.; Yuan, J.; Sonke, J. E.; Zhang, Y.; Zhang, T.; Zheng, W.; Chen, S.; Meng, M.; Chen, J.; Liu, Y.; Peng, X.; Liu, C. Methylmercury Produced in Upper Oceans Accumulates in Deep Mariana Trench Fauna. *Nat. Commun.* **2020**, *11*, 3389.

- (37) Slemr, F.; Angot, H.; Dommergue, A.; Magand, O.; Barret, M.; Weigelt, A.; Ebinghaus, R.; Brunke, E.-G.; Pfaffhuber, K. A.; Edwards, G.; Howard, D.; Powell, J.; Keywood, M.; Wang, F. Comparison of Mercury Concentrations Measured at Several Sites in the Southern Hemisphere. *Atmos. Chem. Phys.* **2015**, *15*, 3125–3133.
- (38) Amin, S.; Asif, T.; Khan, M.; Usinowicz, E.; Mitra, D.; Asaduzzaman, A. Structural, Energetic and Vibrational Properties of Oxidized Mercury in the Gas and Aqueous Phases. *Comput. Theor. Chem.* **2021**, *1198*, 113186.
- (39) Kirk, J. L.; St. Louis, V. L.; Hintelmann, H.; Lehnherr, I.; Else, B.; Poissant, L. Methylated Mercury Species in Marine Waters of the Canadian High and Sub Arctic. *Environ. Sci. Technol.* **2008**, *42*, 8367–8373.
- (40) Constant, P.; Poissant, L.; Villemur, R.; Yumvihoze, E.; Lean, D. Fate of Inorganic Mercury and Methyl Mercury within the Snow Cover in the Low Arctic Tundra on the Shore of Hudson Bay (Québec, Canada). *J. Geophys. Res.* **2007**, *112*, D08309.
- (41) Gionfriddo, C. M.; Tate, M. T.; Wick, R. R.; Schultz, M. B.; Zemla, A.; Thelen, M. P.; Schofield, R.; Krabbenhoft, D. P.; Holt, K. E.; Moreau, J. W. Microbial Mercury Methylation in Antarctic Sea Ice. *Nat. Microbiol.* **2016**, *1*, 16127.
- (42) Larose, C.; Dommergue, A.; De Angelis, M.; Cossa, D.; Averty, B.; Marusczak, N.; Soumis, N.; Schneider, D.; Ferrari, C. Springtime Changes in Snow Chemistry Lead to New Insights into Mercury Methylation in the Arctic. *Geochim. Cosmochim. Acta* **2010**, *74*, 6263–6275.
- (43) Lehnherr, I.; St. Louis, V. L.; Hintelmann, H.; Kirk, J. L. Methylation of Inorganic Mercury in Polar Marine Waters. *Nat. Geosci.* **2011**, *4*, 298–302.
- (44) Bernhoft, R. A. Mercury Toxicity and Treatment: A Review of the Literature. *J. Environ. Public Health* **2012**, *2012*, 460508.
- (45) Asaduzzaman, A.; Riccardi, D.; Afaneh, A. T.; Cooper, S. J.; Smith, J. C.; Wang, F.; Parks, J. M.; Schreckenbach, G. Environmental Mercury Chemistry In Silico. *Acc. Chem. Res.* **2019**, *52*, 379–388.
- (46) Francés-Monerris, A.; Carmona-García, J.; Acuña, A. U.; Dávalos, J. Z.; Cuevas, C. A.; Kinnison, D. E.; Francisco, J. S.; Saiz-Lopez, A.; Roca-Sanjuán, D. Photodissociation Mechanisms of Major Mercury(II) Species in the Atmospheric Chemical Cycle of Mercury. *Angew. Chem. Int. Ed.* **2020**, *59*, 7605–7610.
- (47) Shah, V.; Jacob, D. J.; Thackray, C. P.; Wang, X.; Sunderland, E. M.; Dibble, T. S.; Saiz-Lopez, A.; Černušák, I.; Kellö, V.; Castro, P. J.; Wu, R.; Wang, C. Improved Mechanistic Model of the Atmospheric Redox Chemistry of Mercury. *Environ. Sci. Technol.* **2021**, *55*, 14445–14456.
- (48) Li, X.; Yan, M.; Dibble, T. S.; Zhang, L. Reaction Mechanism and Kinetics of the Important but Neglected Reaction of Hg with NO₂ at Low Temperature. *Chem. Engineering J.* **2022**, *432*, 134373.
- (49) Lam, K. T.; Wilhelmsen, C. J.; Schwid, A. C.; Jiao, Y.; Dibble, T. S. Computational Study on the Photolysis of BrHgONO and the Reactions of BrHgO* with CH₄, C₂H₆, NO, and NO₂: Implications for Formation of Hg(II) Compounds in the Atmosphere. *J. Phys. Chem. A* **2019**, *123*, 1637–1647.
- (50) Dibble, T. S.; Tetu, H. L.; Jiao, Y.; Thackray, C. P.; Jacob, D. J. Modeling the OH-Initiated Oxidation of Mercury in the Global Atmosphere without Violating Physical Laws. *J. Phys. Chem. A* **2020**, *124*, 444–453.

- (51) Dibble, T. S.; Zelie, M. J.; Jiao, Y. Quantum Chemistry Guide to PTRMS Studies of As-Yet Undetected Products of the Bromine-Atom Initiated Oxidation of Gaseous Elemental Mercury. *J. Phys. Chem. A* **2014**, *118*, 7847–7854.
- (52) Khiri, D.; Louis, F.; Černušák, I.; Dibble, T. S. BrHgO '+ CO: Analogue of OH + CO and Reduction Path for Hg(II) in the Atmosphere. *ACS Earth Space Chem.* **2020**, *4*, 1777–1784.
- (53) Wilcox, J.; Okano, T. Ab Initio-Based Mercury Oxidation Kinetics via Bromine at Postcombustion Flue Gas Conditions. *Energy Fuels* **2011**, *25*, 1348–1356.
- (54) Horowitz, H. M.; Jacob, D. J.; Zhang, Y.; Dibble, T. S.; Slemr, F.; Amos, H. M.; Schmidt, J. A.; Corbitt, E. S.; Marais, E. A.; Sunderland, E. M. A New Mechanism for Atmospheric Mercury Redox Chemistry: Implications for the Global Mercury Budget. *Atmos. Chem. Phys.* **2017**, *17*, 6353–6371.
- (55) Balabanov, N. B.; Peterson, K. A. A Systematic *Ab Initio* Study of the Structure and Vibrational Spectroscopy of HgCl₂, HgBr₂, and HgBrCl. *J. Chem. Phys.* **2003**, *119*, 12271–12278.
- (56) Balabanov, N. B.; Peterson, K. A. Mercury and Reactive Halogens: The Thermochemistry of Hg + {Cl₂, Br₂, BrCl, ClO, and BrO}. *J. Phys. Chem. A* **2003**, *107*, 7465–7470.
- (57) Saiz-Lopez, A.; Acuña, A. U.; Trabelsi, T.; Carmona-García, J.; Dávalos, J. Z.; Rivero, D.; Cuevas, C. A.; Kinnison, D. E.; Sitkiewicz, S. P.; Roca-Sanjuán, D.; Francisco, J. S. Gas-Phase Photolysis of Hg(I) Radical Species: A New Atmospheric Mercury Reduction Process. *J. Am. Chem. Soc.* **2019**, *141*, 8698–8702.
- (58) Vogelsong, L.; Fuentes, J. D.; Asaduzzaman, A. Deposition and Reduction of Oxidized Mercury on the Ice Surface: Quantum-Chemical Study and Implication of Mercury Activities in the Arctic. *J. Phys. Chem. C* **2023**, *127*, 2657-2665.
- (59) Kresse, G.; Hafner, J. Norm-Conserving and Ultrasoft Pseudopotentials for First-Row and Transition Elements. *J. Phys.: Condens. Matter* **1994**, *6*, 8245–8257.
- (60) Kresse, G.; Furthmüller, J. Efficiency of Ab-Initio Total Energy Calculations for Metals and Semiconductors Using a Plane-Wave Basis Set. *Comput. Mater. Sci.* **1996**, *6*, 15–50.
- (61) Kresse, G.; Joubert, D. From Ultrasoft Pseudopotentials to the Projector Augmented-Wave Method. *Phys. Rev. B* **1999**, *59*, 1758–1775.
- (62) Perdew, J. P.; Burke, K.; Ernzerhof, M. Generalized Gradient Approximation Made Simple. *Phys. Rev. Lett.* **1996**, *77*, 3865–3868.
- (63) Monkhorst, H. J.; Pack, J. D. Special Points for Brillouin-Zone Integrations. *Phys. Rev. B* **1976**, *13*, 5188–5192.
- (64) Goto, A.; Hondoh, T.; Mae, S. The Electron Density Distribution in Ice I_h Determined by Single-crystal X-ray Diffractometry. *J. Chem. Phys.* **1990**, *93*, 1412–1417.
- (65) Estrin, D. A.; Paglieri, L.; Corongiu, G.; Clementi, E. Small Clusters of Water Molecules Using Density Functional Theory. *J. Phys. Chem.* **1996**, *100*, 8701–8711.
- (66) Miró, P.; Cramer, C. J. Water Clusters to Nanodrops: A Tight-Binding Density Functional Study. *Phys. Chem. Chem. Phys.* **2013**, *15*, 1837–1843.
- (67) Zhang, L.; Li, W.; Fang, T.; Li, S. Accurate Relative Energies and Binding Energies of Large Ice–Liquid Water Clusters and Periodic Structures. *J. Phys. Chem. A* **2017**, *121*, 4030–4038.
- (68) Tossell, J. A. Calculation of the Energetics for the Oligomerization of Gas Phase HgO and HgS and for the Solvolysis of Crystalline HgO and HgS. *J. Phys. Chem. A* **2006**, *110*, 2571–2578.

- (69) Asaduzzaman, A.; Schreckenbach, G. Chalcogenophilicity of Mercury. *Inorg. Chem.* **2011**, *50*, 3791–3798.
- (70) Asaduzzaman, A. Md.; Wang, F.; Schreckenbach, G. Quantum-Chemical Study of the Diffusion of Hg(0, I, II) into the Ice(Ih). *J. Phys. Chem. C* **2012**, *116*, 5151–5154.
- (71) Asaduzzaman, A. Md.; Schreckenbach, G. Adsorption of Na and Hg on the Ice(Ih) Surface: A Density-Functional Study. *J. Phys. Chem. C* **2010**, *114*, 2941–2946.
- (72) Asaduzzaman, A. M.; Zega, T. J.; Laref, S.; Runge, K.; Deymier, P. A.; Muralidharan, K. A Computational Investigation of Adsorption of Organics on Mineral Surfaces: Implications for Organics Delivery in the Early Solar System. *Earth Planet. Sci. Lett.* **2014**, *408*, 355–361.
- (73) Peterson, K. A.; Shepler, B. C.; Figgen, D.; Stoll, H. On the Spectroscopic and Thermochemical Properties of ClO, BrO, IO, and Their Anions. *J. Phys. Chem. A* **2006**, *110*, 13877–13883.
- (74) Jiao, Y.; Dibble, T. S. Structures, Vibrational Frequencies, and Bond Energies of the BrHgOX and BrHgXO Species Formed in Atmospheric Mercury Depletion Events. *J. Phys. Chem. A* **2017**, *121*, 7976–7985.
- (75) Jiao, Y.; Dibble, T. S. Quality Structures, Vibrational Frequencies, and Thermochemistry of the Products of Reaction of BrHg* with NO₂, HO₂, ClO, BrO, and IO. *J. Phys. Chem. A* **2015**, *119*, 10502–10510.
- (76) Castro, L.; Dommergue, A.; Renard, A.; Ferrari, C.; Ramirez-Solis, A.; Maron, L. Theoretical Study of the Solvation of HgCl₂, HgClOH, Hg(OH)₂ and HgCl₃⁻: A Density Functional Theory Cluster Approach. *Phys. Chem. Chem. Phys.* **2011**, *13*, 16772-16779.
- (77) Ramírez-Solís, A.; Maron, L. Nonharmonic Vibrational Effects in HgClOH: An MP2 Born-Oppenheimer Molecular Dynamics Study. *Int. J. Quantum Chem.* **2012**, *112*, 3484–3489.
- (78) Asaduzzaman, A. Md.; Schreckenbach, G. Computational Studies of the Interactions of I⁻ and I₃⁻ with TiO₂ Clusters: Implications for Dye-Sensitized Solar Cells. *Theor. Chem. Acc.* **2011**, *129*, 199–208.
- (79) Malloum, A.; Fifen, J. J.; Dhaouadi, Z.; Nana Engo, S. G.; Conradie, J. Structures, Relative Stability and Binding Energies of Neutral Water Clusters, (H₂O)_{2–30}. *New J. Chem.* **2019**, *43*, 13020–13037.
- (80) Su, J. T.; Xu, X.; Goddard, W. A. Accurate Energies and Structures for Large Water Clusters Using the X3LYP Hybrid Density Functional. *J. Phys. Chem. A* **2004**, *108*, 10518–10526.
- (81) Holmes, J. D.; Otero-de-la-Roza, A.; DiLabio, G. A. Accurate Modeling of Water Clusters with Density-Functional Theory Using Atom-Centered Potentials. *J. Chem. Theory Comput.* **2017**, *13*, 4205–4215.
- (82) Taamalli, S.; Pitoňák, M.; Dibble, T. S.; Černušák, I.; Louis, F. Theoretical Study of the Monohydration of Mercury Compounds of Atmospheric Interest. *J. Phys. Chem. A* **2021**, *125*, 5819–5828.
- (83) Yi, Y. S.; Han, Y.; Hur, S. D. Reductive Adsorption of Atmospheric Oxidized Mercury on Ice: Insights from Density Functional Calculations. *ACS Earth Space Chem.* **2021**, *5*, 3170–3181.

TOC Graphic

